

Functional auditory hair cells produced in the mammalian cochlea by *in utero* gene transfer

Samuel P. Gubbels^{1*†}, David W. Woessner^{1*†}, John C. Mitchell², Anthony J. Ricci³ & John V. Brigande¹

Sensory hair cells in the mammalian cochlea convert mechanical stimuli into electrical impulses that subserve audition^{1,2}. Loss of hair cells and their innervating neurons is the most frequent cause of hearing impairment³. Atonal homologue 1 (encoded by *Atoh1*, also known as *Math1*) is a basic helix–loop–helix transcription factor required for hair-cell development^{4–6}, and its misexpression *in vitro*^{7,8} and *in vivo*^{9,10} generates hair-cell-like cells. *Atoh1*-based gene therapy to ameliorate auditory¹⁰ and vestibular¹¹ dysfunction has been proposed. However, the biophysical properties of putative hair cells induced by *Atoh1* misexpression have not been characterized. Here we show that *in utero* gene transfer of *Atoh1* produces functional supernumerary hair cells in the mouse cochlea. The induced hair cells display stereociliary bundles, attract neuronal processes and express the ribbon synapse marker carboxy-terminal binding protein 2 (refs 12,13). Moreover, the hair cells are capable of mechano-electrical transduction^{1,2} and show basolateral conductances with age-appropriate specializations. Our results demonstrate that manipulation of cell fate by transcription factor misexpression produces functional sensory cells in the postnatal mammalian cochlea. We expect that our *in utero* gene transfer paradigm will enable the design and validation of gene therapies to ameliorate hearing loss in mouse models of human deafness^{14,15}.

We devised an *in utero* gene transfer method to conduct gain-of-function studies in the developing mouse inner ear¹⁶ (Fig. 1 and Supplementary Figs 1 and 2). A plasmid consisting of the human elongation factor 1- α gene (*EEF1A1*; also known as *EF1A*) promoter¹⁷ driving the expression of a destabilized form (2 h half-life) of green fluorescent protein (ZsGreen)^{18,19} was microinjected through the uterus into the fluid-filled cavity of the embryonic day 11.5 (E11.5) mouse otic vesicle (Fig. 1a and Supplementary Video 1). The plasmid-filled left otocyst was centred in the field of a paddle-style circular electrode, and a directional square-wave pulse train was delivered to electroporate ventral progenitor cells that give rise to the organ of Corti (Fig. 1b and Supplementary Video 2). ZsGreen was detected 24 h after electroporation in a teardrop-shaped pattern consistent with the morphology of the otocyst (four of six otocysts; Fig. 1c and Supplementary Fig. 2). Histological analysis revealed ZsGreen-positive progenitor cells in their stereotyped pseudostratified arrangement within the otic epithelium (Fig. 1d)²⁰. These data indicate that *in vivo* electroporation transfects otic epithelial progenitor cells in the ventromedial otocyst and produces robust transgene expression within 24 h.

To determine which differentiated cell types arise from transfected otic progenitors, we injected and electroporated EF1 α -enhanced

green fluorescent protein (GFP) at E11.5 and analysed E18.5 cochlear whole mounts immunostained for the hair-cell marker myosin 7a (*Myo7a*)^{21,22}. The gross morphology of the inner ear at E18.5 was unaffected, and electroporated embryos carried to term had normal auditory function one month after birth (Supplementary Table 1). Robust GFP expression was present in inner and outer hair cells and supporting cells in the organ of Corti at E18.5 (Fig. 2a, b, d, f and

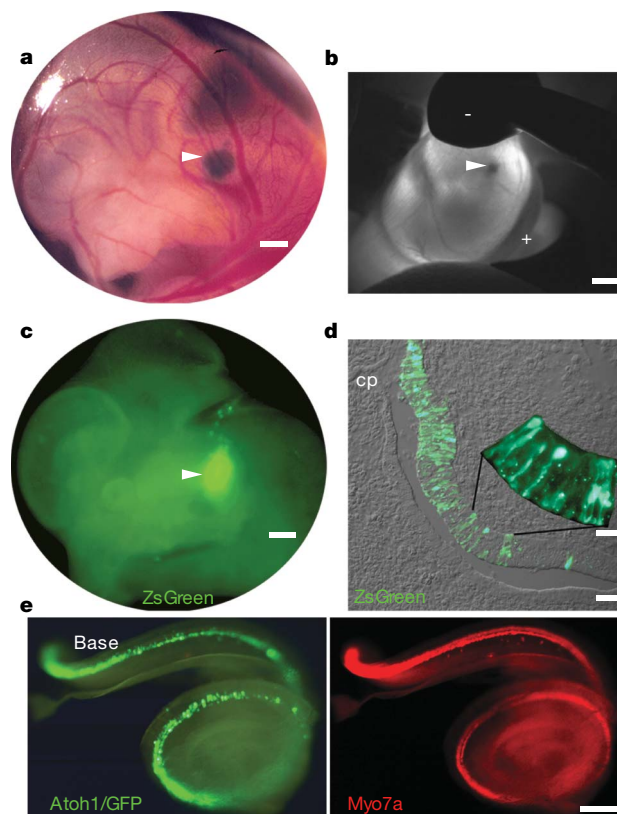


Figure 1 | *In utero* gene transfer to the developing mouse inner ear.

a, Expression plasmid was microinjected into the E11.5 otic vesicle. **b**, The vesicle was centred between the cathode (–) and anode (+) and electroporated. **c**, Destabilized GFP (ZsGreen) was expressed in the otic territory 24 h after electroporation. **d**, E12.5 progenitors in the medial and ventral otic epithelium expressed ZsGreen robustly. **e**, E18.5 *Atoh1*/GFP-transfected cochlea (left) immunostained for *Myo7a* (right). Arrowheads indicate left otocyst. cp, lateral canal plate; scale bars, 200 μ m (**a**); 500 μ m (**b**, **c**); 50 μ m (**d**); 10 μ m (**d**, inset); 100 μ m (**e**).

¹Department of Otolaryngology, Oregon Hearing Research Center, and ²Department of Restorative Dentistry, Division of Biomaterials and Biomechanics, School of Dentistry, Oregon Health & Science University, 3181 SW Sam Jackson Park Road, Portland, Oregon 97239, USA. ³Department of Otolaryngology-Head and Neck Surgery, Stanford University School of Medicine, 801 Welch Road, Stanford, California 94305, USA. [†]Present addresses: Department of Surgery, Division of Otolaryngology, University of Wisconsin – Madison, K4/719 CSC, 600 Highland Avenue, Madison, Wisconsin 53792, USA (S.P.G.); Department of Pharmacology and Toxicology, University of Utah, College of Pharmacy, 30 South 2000 East, Room 201, Salt Lake City, Utah 84112, USA (D.W.W.).

*These authors contributed equally to this work.

Supplementary Fig. 3). The distribution of transfected cells in the cochlea was constrained to the organ of Corti proper. Differential regulation of GFP expression by the *EEF1A1* promoter may account for this restricted pattern. These data indicate that *in vivo* electroporation transfects otic progenitors that give rise to all of the constituent cell types within the organ of Corti but it does not adversely affect gross embryonic development or the postnatal acquisition of hearing.

To induce otic epithelial progenitor cells to adopt a hair-cell fate, we misexpressed *Atoh1*, a basic helix–loop–helix transcription factor

required for hair-cell formation⁴. A plasmid generating a bicistronic message encoding *Atoh1* and enhanced GFP was injected and electroporated in the E11.5 otocyst. The gross distribution of *Atoh1*/GFP expression in the E18.5 cochlea seemed to follow that defined by *Myo7a* (Fig. 1e), suggesting that progenitors giving rise to the organ of Corti were transfected with *Atoh1*. *Atoh1*/GFP⁺ cells co-expressing *Myo7a* were present in the base, midbase and apex of transfected cochleae (Fig. 2c, e, g). The stereotyped pattern of one inner and three outer rows of hair cells was altered by the overabundance of *Atoh1*/GFP⁺/*Myo7a*⁺ cells that we refer to as supernumerary cells (Fig. 2c, e, g). The apical surfaces of the supernumerary cells had phalloidin-positive epithelial protrusions at E18.5 that resembled immature stereociliary bundles (Supplementary Fig. 4a–d), which persisted for one month after birth (Fig. 2h–k). Ectopic *Myo7a*⁺ cells displaced

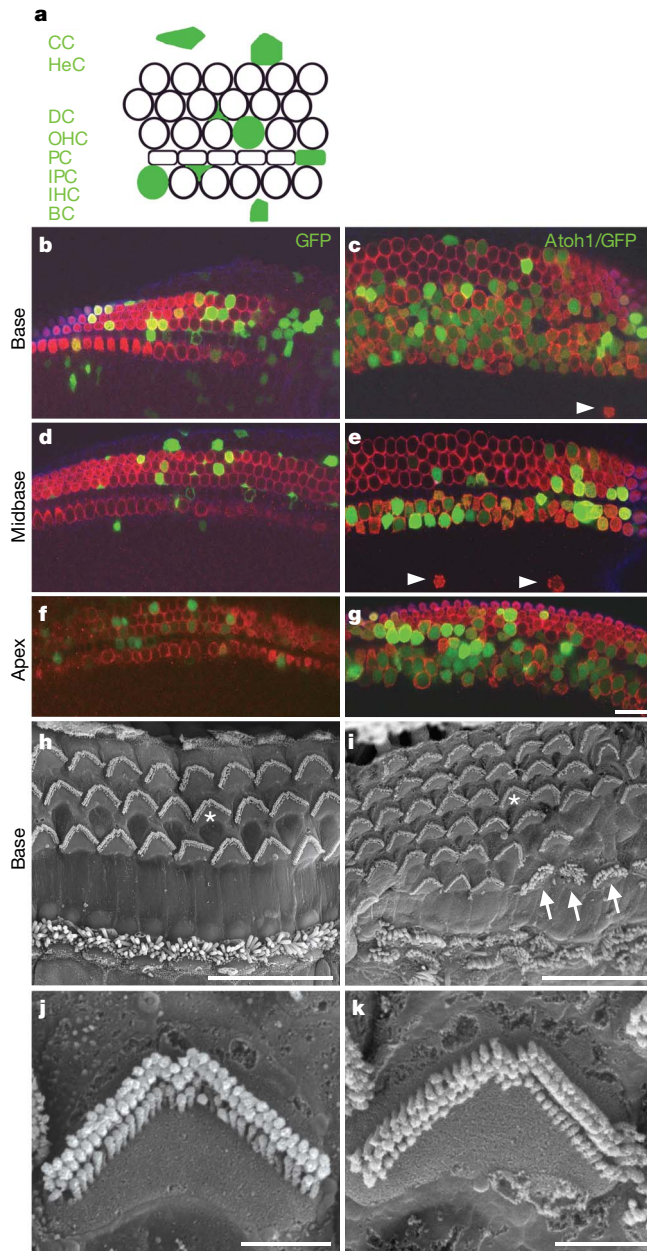


Figure 2 | *Atoh1* misexpression generates supernumerary *Myo7a*⁺ cells bearing stereociliary bundles. **a**, Schematic diagram of cell types in the organ of Corti transfected with *Atoh1*/enhanced GFP (filled green): CC, Claudius's cells; HeC, Hensen's cells; DC, Deiters's cells; OHC, outer hair cell; PC, pillar cell; IPC, inner phalangeal cell; BC, border cell. **b–g**, Laser confocal micrographs of E18.5 GFP-transfected (**b, d, f**) and *Atoh1*/GFP-transfected (**c, e, g**) organs of Corti immunostained for *Myo7a* (red). All of the *Atoh1*/GFP⁺ cells in **c, e** and **g** are *Myo7a*⁺. **h–j**, scanning electron micrographs of postnatal day 35, untransfected (**h**) and *Atoh1*/GFP-transfected (**i**) organs of Corti. Asterisks in **h** and **i** indicate stereociliary bundles imaged at higher magnification in **j** and **k**, respectively. The arrows indicate three cells with atypical bundles. Scale bars, 20 μm (**b–i**); 2 μm (**j, k**).

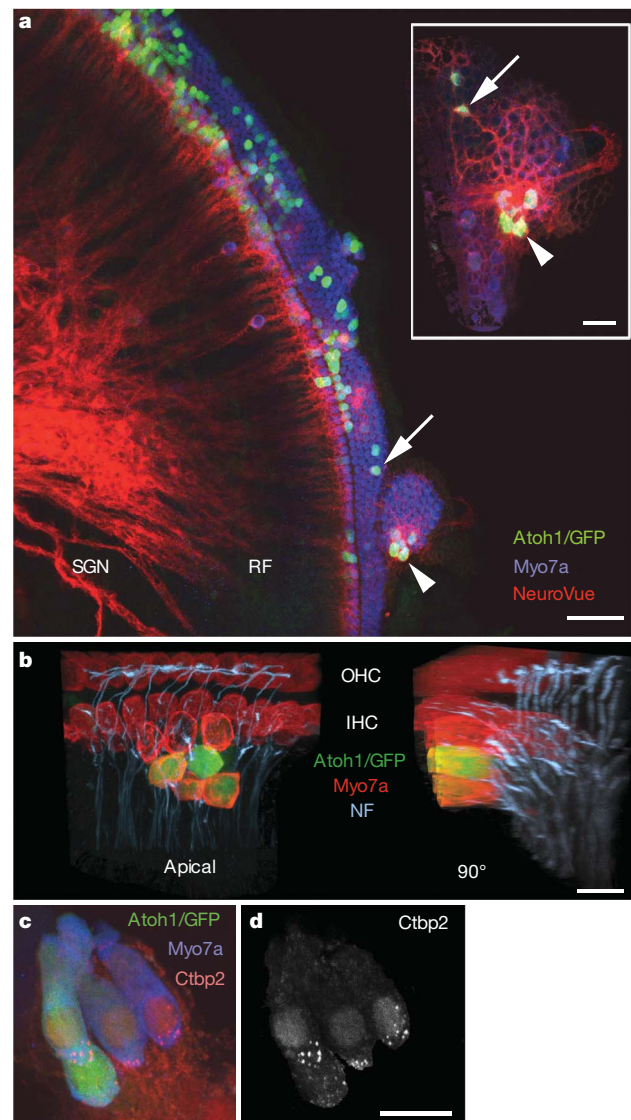


Figure 3 | *Atoh1*/GFP⁺ cells show morphological and molecular correlates of innervation and synaptogenesis. **a**, NeuroVue-Red placed in the cochlear nucleus labels radial fibers (RF) of spiral ganglion neurons (SGN) that project to *Atoh1*/GFP⁺/*Myo7a*⁺ cells (arrow and arrowhead). Inset, basal regions of indicated cells. **b**, Neurofilament-positive (NF⁺) processes associate with *Myo7a*⁺ inner and outer hair cells (apical). NF⁺ processes terminated at the base of an *Atoh1*/GFP⁺/*Myo7a*⁺ cell cluster as seen in the 90° rotation of the apical three-dimensional reconstruction. **c**, *Ctbp2* (red) was localized to the basolateral domain at P35. **d**, The *Ctbp2* (red) signal in **c** that was contained within the *Myo7a*⁺ hair-cell cytoplasm. Scale bars, 50 μm (**a**); 20 μm (**a**, inset); 10 μm (**b–d**).

from the organ of Corti towards the modiolus were occasionally observed (Fig. 2c, e, and Supplementary Fig. 4f).

The total number of Myo7a⁺ cells (that is, putative hair cells, whether transfected or not) in the cochlear base was increased 1.8-fold, and 50% of these cells were Atoh1/GFP⁺ (Supplementary Table 2). In addition, we detected a 2.2-fold increase in putative inner hair cells (IHCs) and a 1.5-fold increase in putative outer hair cells (OHCs) in the base. Consequently, the ratio of OHC to IHC shifted from 3.4:1 to 2.4:1 as a result of the disproportionate increase in IHCs. Little is known about inner and outer hair-cell fate specification and whether the cues responsible are temporally or spatially regulated (or both). *In utero* gene transfer of *Atoh1* at different stages of otic vesicle development may provide insights into the molecular mechanisms governing hair-cell fate specification.

There were fewer supernumerary Myo7a⁺ cells generated in the midbase (1.2-fold increase; 40% Atoh1/GFP⁺), and none in the apex (Supplementary Table 2). The observed base-to-apex gradation in the abundance of supernumerary Myo7a⁺ cells is inversely associated with the gradient of cell cycle exit in the organ of Corti, in which apical progenitors exit from the cell cycle first and basal progenitors exit last²³. We propose that the large increase in supernumerary hair cells in the base results from clonal expansion of *Atoh1*-transfected progenitors.

To test whether the supernumerary Atoh1/GFP⁺/Myo7a⁺ cells attracted nerve fibres, we labelled neurons in the cochlear nucleus in retrograde fashion²⁴ and analysed the distribution of labelled processes to the organ of Corti. A cluster of four Atoh1/GFP⁺/Myo7a⁺ cells in the OHC region attracted a cluster of fibres that labelled with NeuroVue Red²⁵ (Fig. 3a, arrowhead) whose density was enriched at the base of the cluster (Fig. 3a, inset, arrowhead). An isolated Atoh1/GFP⁺ cell in the same organ of Corti (Fig. 3a, arrow) attracted a refined NeuroVue-positive fibre to its base (Fig. 3a, inset, arrow). To confirm that the labelled fibres were neuronal processes, we analysed neurofilament distribution in Atoh1/GFP-transfected cochleae. We detected neurofilament-positive processes terminating at the base of both untransfected Myo7a⁺ cells and Atoh1/GFP⁺/Myo7a⁺ cells (Fig. 3b and Supplementary Video 3). We next sought to determine whether the Atoh1/GFP-transfected cells expressed carboxy-terminal binding protein 2 (Ctbp2), a marker of the hair-cell ribbon synapse, at postnatal day 35 (P35). We detected discrete foci of Ctbp2 in the basolateral domain in 20 of 39 Atoh1/GFP⁺ cells from two cochleae (Fig. 3c, d, and Supplementary Video 4). These data suggest that Atoh1/GFP⁺ cells engage a synaptogenic program and are innervated by neurons that associate with the cochlear nucleus.

Hair cells convert mechanical stimuli into electrical impulses and have a distinct set of biophysical properties. To characterize the identity of Atoh1/GFP⁺ cells further, we interrogated their electrophysiological properties at P4–P6. Cells were selected and grouped on the basis of whether they were GFP⁺ or GFP⁻ and whether they had the morphological phenotype of an IHC or an OHC. Morphology was based on the shape of the hair bundle viewed by differential interference contrast microscopy, with OHCs having the classical V shape and the IHCs being straight. OHCs were located on the strial side of pillar cells and IHCs were located on the modiolar side (Fig. 2a). Supernumerary IHCs and OHCs were investigated. The ectopic cells displaced towards the modiolus were structurally unstable and could not be patch-clamped (Supplementary Fig. 4f). Comparisons were made both between cell types and within types for GFP⁺ and GFP⁻ cells. Where no differences were observed, data were pooled.

No difference was observed in zero-current potential between GFP⁺ and GFP⁻ hair cells, or between IHCs and OHCs, with values of -63 ± 13 mV ($n = 5$) and -49 ± 15 mV ($n = 7$), respectively. Although membrane capacitance was not different between GFP⁺ and GFP⁻ cells, capacitance was different ($P < 0.001$, two-tailed t -test) between IHCs and OHCs, with values of 7.3 ± 1.3 pF ($n = 11$) and 4.7 ± 1.5 pF ($n = 24$), respectively. These results indicate that Atoh1/GFP-transfected and untransfected cells elaborated

differential capacitances consistent with their identities as inner or outer hair cells.

Mechanotransduction was investigated by stimulating hair bundles with a piezoelectrically driven glass fibre (Fig. 4a)²⁶. We found that hair cells induced by *Atoh1* misexpression had the same range of current amplitudes, sensitivity and adaptation as hair cells not expressing GFP. Figure 4 shows this analysis for GFP⁺ and GFP⁻ OHCs. Current amplitudes varied considerably as expected, in part because of the developmental age at which they were measured²⁶. Peak currents of 152 ± 107 pA ($n = 15$) and 200 ± 177 pA ($n = 7$) were measured for GFP⁺ and GFP⁻ cells, respectively (Fig. 4b, c). Normalized current–displacement plots (Fig. 4d) were fitted with a single Boltzmann function, and no differences were found either in half activating displacement or in sensitivity, with values of 0.54 ± 0.06 μm and 0.53 ± 0.02 μm and slopes of 0.17 ± 0.05 μm^{-1} and 0.17 ± 0.03 μm^{-1} ($r^2 = 0.99$ for both) for GFP⁺ and GFP⁻ cells, respectively. Adaptation kinetics were compared by fitting the response to a positive stimulus that elicited less than 50% of the maximal response with the equation for a double exponential²⁷. Fast and slow time constants did not differ between groups and gave values of 0.81 ± 0.48 ms ($n = 6$) and 0.39 ± 0.3 ms ($n = 4$) for the fast time constant and 8 ± 10 ms and 8 ± 6 ms for the slow time constant for GFP⁺ and GFP⁻ OHCs, respectively. These results suggest that mechanotransduction follows a normal developmental progression in Atoh1/GFP⁺ hair cells²⁶.

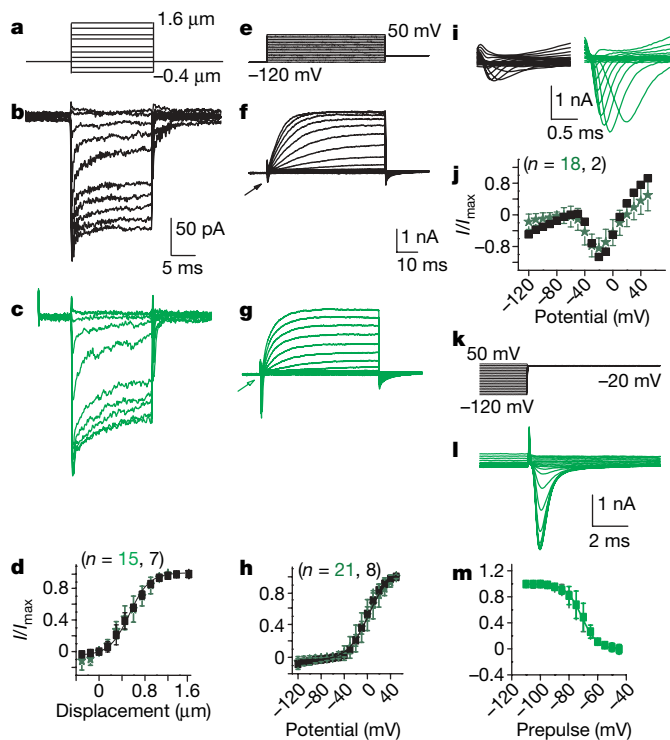


Figure 4 | Atoh1/GFP⁺ cells mechanotransduce and elaborate age-appropriate basolateral conductances. **a**, Biophysical response properties of control (black) and GFP⁺ (green) hair cells. **b**, **c**, Mechanically evoked currents from a holding potential of -84 mV elicited from the stimulus in **a**. **d**, Normalized peak current against displacement; the solid line is a Boltzmann fit. **f**, **g**, Current responses to the voltage-clamp stimuli in **e** for control (**f**) and GFP⁺ (**g**) hair cells. **h**, Steady-state current–voltage plot from the data in **f** and **g**; the solid line is a Boltzmann fit. **i**, Expanded current traces from the regions indicated by the arrows in **f** and **g**. **j**, Plot of normalized peak current against potential for inward current. **k**, Stimulus protocol to probe inactivation that elicited currents in **l**. **m**, Prepulse potential against normalized peak inward current; the solid line is a Boltzmann fit. Data are presented as means \pm s.d., and two-tailed t -tests were used for statistical comparisons.

Basolateral conductances were also investigated (Fig. 4e–m). A voltage protocol (Fig. 4e) that first prepulsed the potential from -84 mV to -120 mV for 200 ms was used to determine whether inactivating conductances were present. Both inward and outward currents were observed (Fig. 4f, g, i). The outward currents did not vary in current amplitude or activation properties between GFP⁺ and GFP⁻ cells; however, there was a difference ($P < 0.001$) between OHCs and IHCs in current amplitude, with OHCs having a peak current of $1,878 \pm 653$ pA ($n = 29$) and IHCs having a peak current of $2,790 \pm 767$ pA ($n = 14$). These results again demonstrate that Atoh1/GFP⁺ cells develop outward current characteristics consistent with their terminal differentiation as inner or outer hair cells.

Rapidly activating, rapidly inactivating inward currents were observed in 90% of the GFP⁺ OHCs but in only 30% of GFP⁻ cells (Fig. 4f, g, i–m). The trend was less apparent for IHCs, with 80% of GFP⁺ and 66% of GFP⁻ IHCs having inward currents. The greatest difference in the inward current is shown in Fig. 4i; the GFP⁺ OHCs had much larger current amplitudes than the GFP⁻ cells did, with peak currents of $1,998 \pm 1,178$ pA ($n = 19$) and 475 ± 100 pA ($n = 3$), respectively ($P < 0.05$). Persistent, strong expression of Atoh1/GFP at postnatal stages by the *EEF1A1* promoter may underlie the difference in current amplitude observed. No difference was found in activation properties between any of the groups. Inactivation was not different between GFP⁺ and GFP⁻ cells, but again there was a difference in the half inactivation between GFP⁺ IHCs and OHCs, with values of -78 ± 1 mV and -71 ± 1 mV, respectively ($P < 0.01$, $n = 4$ for each). No difference was found for the slope, with values of 6.0 ± 1 mV⁻¹ and 5.5 ± 0.4 mV⁻¹ for IHCs and OHCs, respectively. These data support the conclusion that misexpression of *Atoh1* leads to the production of functional sensory hair cells in the postnatal cochlea that elaborate electrophysiological specializations consistent with inner or outer hair-cell identity.

There is close interest in gene^{10,11} and cell^{28,29} replacement strategies to restore auditory and vestibular function in the diseased inner ear. Although *Atoh1* misexpression in cochlear cultures^{7,8} and in the adult guinea pig inner ear^{9,10} generates cells with some of the morphological and molecular characteristics of sensory hair cells, no electrophysiological analysis of the induced hair cells was conducted in previous studies. We microinjected an expression plasmid encoding Atoh1 into the nascent mouse otocyst and subsequently transfected otic epithelial progenitor cells by *in vivo* electroporation. The induced supernumerary hair cells express Myo7a, attract neurofilament-bearing processes and localize the ribbon synapse marker Ctbp2 to their basolateral domain. In addition, the induced hair cells mechanotransduce and possess basolateral currents consistent with their maturational stage. Our work establishes that supernumerary cells induced by electroporation-mediated gene transfer of *Atoh1* are functional sensory hair cells. The ability to conduct gain-of-function experiments in the developing mammalian inner ear by gene transfer *in utero* may permit the design and functional assessment of gene therapies aimed at ameliorating hearing loss and vestibular dysfunction in mice that model human deafness and balance disorders. This capability is a crucial first step in defining translational therapies to ameliorate the effects of inner-ear disease in humans.

METHODS SUMMARY

Experimental embryology. Timed pregnant dams were laparotomized to externalize the uterus. Four to six otocysts were injected and electroporated in each dam. Transfected inner ears were harvested at E12.5, E18.5, P4–P6 or P28–P35 and fixed in 4% paraformaldehyde in PBS before cryosectioning, nerve tract tracing, scanning electron microscopy or immunohistochemistry.

Nerve tract tracing. The E18.5 crania were hemisected sagittally, and a nylon filter coated with NeuroVue Red was inserted into the cochlear nucleus followed by incubation for 7 days at 37 °C in PBS/0.1% sodium azide. Nerve tracts were revealed by confocal microscopy in cochlear whole mounts immunostained for Myo7a.

Scanning electron microscopy. The OTOTO method was performed³⁰.

Video. Confocal stacks of immunostained cochleae were processed with Imaris software to generate three-dimensional images and video.

Cell quantification. The base, midbase and apex of transfected E18.5 cochleae immunostained for Myo7a were imaged by confocal microscopy. The mean number of hair cells, transfected hair cells and transfected supporting cells was counted per 100 μ m field (mean \pm s.e.m.), and the Mann–Whitney *U*-test was used for statistical comparisons.

Electrophysiology. Hair cells were patch-clamped with an axoclamp 200b amplifier coupled to a 1322 digitdata A/D, D/A board driven by JClamp software. Soda-glass pipettes (resistances 1–3 M Ω) coated with ski wax were used to record from both GFP⁺ and GFP⁻ cells. Mechanical stimulation was accomplished with a stiff glass probe attached to a piezoelectric stack. Stimuli were filtered at 20 kHz and differentially amplified through an attenuator to regulate stimulus amplitudes. Data were sampled at 40 kHz and filtered at 10 kHz; each stimulus is an average of eight samples. Junction potential and series resistance were corrected offline. No leak subtraction was applied. Data are presented as means \pm s.d., and two-tailed *t*-tests were used for statistical comparisons.

Full Methods and any associated references are available in the online version of the paper at www.nature.com/nature.

Received 1 April; accepted 17 July 2008.

Published online 27 August 2008.

- Vollrath, M., Kwan, K. & Corey, D. The micromachinery of mechanotransduction in hair cells. *Annu. Rev. Neurosci.* **30**, 339–365 (2007).
- Grant, L. & Fuchs, P. A. Auditory transduction in the mouse. *Pflugers Arch.* **454**, 793–804 (2007).
- Davis, A. in *Hearing Science and Hearing Disorders* (eds Lutman, M. & Haggard, M.) (Academic, 1993).
- Birmingham, N. A. *et al.* *Math1*: an essential gene for the generation of inner ear hair cells. *Science* **284**, 1837–1841 (1999).
- Chen, P., Johnson, J. E., Zoghbi, H. Y. & Segil, N. The role of *Math1* in inner ear development: Uncoupling the establishment of the sensory primordium from hair cell fate determination. *Development* **129**, 2495–2505 (2002).
- Jones, J. M. *et al.* Inhibitors of differentiation and DNA binding (Ids) regulate *Math1* and hair cell formation during the development of the organ of Corti. *J. Neurosci.* **26**, 550–558 (2006).
- Zheng, J. L. & Gao, W. Q. Overexpression of *Math1* induces robust production of extra hair cells in postnatal rat inner ears. *Nature Neurosci.* **3**, 580–586 (2000).
- Woods, C., Montcouquiol, M. & Kelley, M. W. *Math1* regulates development of the sensory epithelium in the mammalian cochlea. *Nature Neurosci.* **7**, 1310–1318 (2004).
- Kawamoto, K. *et al.* *Math1* gene transfer generates new cochlear hair cells in mature guinea pigs *in vivo*. *J. Neurosci.* **23**, 4395–4400 (2003).
- Izumikawa, M. *et al.* Auditory hair cell replacement and hearing improvement by *Atoh1* gene therapy in deaf mammals. *Nature Med.* **11**, 271–276 (2005).
- Staecker, H., Praetorius, M., Baker, K. & Brough, D. E. Vestibular hair cell regeneration and restoration of balance function induced by *math1* gene transfer. *Otol. Neurotol.* **28**, 223–231 (2007).
- Knirsch, M. *et al.* Persistence of Ca_v1.3 Ca²⁺ channels in mature outer hair cells supports outer hair cell afferent signaling. *J. Neurosci.* **27**, 6442–6451 (2007).
- Wan, L., Almers, W. & Chen, W. Two *ribeye* genes in teleosts: the role of *Ribeye* in ribbon formation and bipolar cell development. *J. Neurosci.* **25**, 941–949 (2005).
- Brown, S. D., Hardisty-Hughes, R. E. & Mburu, P. Quiet as a mouse: dissecting the molecular and genetic basis of hearing. *Nature Rev. Genet.* **9**, 277–290 (2008).
- Friedman, L. M., Dror, A. A. & Avraham, K. B. Mouse models to study inner ear development and hereditary hearing loss. *Int. J. Dev. Biol.* **51**, 609–631 (2007).
- Gubbels, S., Woessner, D., Mitchell, J. & Brigande, J. in *Thirtieth Annual MidWinter Research Meeting of the Association for Research in Otolaryngology*, 10–15 February 2007 (ed. Santi, P. A.) vol. 30 330 (Association for Research in Otolaryngology, 2007).
- Kim, D. W. *et al.* Use of the human elongation factor 1 α promoter as a versatile and efficient expression system. *Gene* **91**, 217–223 (1990).
- Li, X. *et al.* Generation of destabilized green fluorescent protein as a transcription reporter. *J. Biol. Chem.* **273**, 34970–34975 (1998).
- Rechsteiner, M. PEST sequences are signals for rapid intracellular proteolysis. *Semin. Cell Biol.* **1**, 433–440 (1990).
- Sher, A. E. The embryonic and postnatal development of the inner ear of the mouse. *Acta Otolaryngol., Suppl.* **285**, 1–77 (1971).
- Hasson, T. *et al.* Unconventional myosins in inner ear sensory epithelia. *J. Cell Biol.* **137**, 1287–1307 (1997).
- Hasson, T. *et al.* Expression in cochlea and retina of myosin VIIa, the gene product defective in Usher syndrome type 1B. *Proc. Natl Acad. Sci. USA* **92**, 9815–9819 (1995).
- Chen, P. & Segil, N. p27^{Kip1} links cell proliferation to morphogenesis in the developing organ of Corti. *Development* **126**, 1581–1590 (1999).
- Maklad, A. & Fritzsche, B. Partial segregation of posterior crista and saccular fibers to the nodulus and uvula of the cerebellum in mice, and its development. *Brain Res. Dev. Brain Res.* **140**, 223–236 (2003).
- Fritzsche, B. *et al.* Diffusion and imaging properties of three new lipophilic tracers, NeuroVue Maroon, NeuroVue Red and NeuroVue Green and their use

- for double and triple labeling of neuronal profile. *Brain Res. Bull.* **66**, 249–258 (2005).
26. Waguespack, J., Salles, F. T., Kachar, B. & Ricci, A. J. Stepwise morphological and functional maturation of mechanotransduction in rat outer hair cells. *J. Neurosci.* **27**, 13890–13902 (2007).
 27. Wu, Y. C., Ricci, A. J. & Fettiplace, R. Two components of transducer adaptation in auditory hair cells. *J. Neurophysiol.* **82**, 2171–2181 (1999).
 28. Li, H., Corrales, C. E., Edge, A. & Heller, S. Stem cells as therapy for hearing loss. *Trends Mol. Med.* **10**, 309–315 (2004).
 29. Hu, Z. & Ulfendahl, M. Cell replacement therapy in the inner ear. *Stem Cells Dev.* **15**, 449–459 (2006).
 30. Self, T. *et al.* Shaker-1 mutations reveal roles for myosin VIIA in both development and function of cochlear hair cells. *Development* **125**, 557–566 (1998).

Supplementary Information is linked to the online version of the paper at www.nature.com/nature.

Acknowledgements We thank C. Breese and J. Jungwirth for expert technical support; C. Cepko and G. Nolan for plasmids EF1 α -GFP and BMN-IRES-GFP,

respectively; A. Kiernan, D. Fekete, S. Heller, A. Nguyen-Huynh, C. Breese and J. Jungwirth for critical comments that improved the manuscript; D. Trune, B. Fritzsche and N. Segil for helpful discussions; S. Griest for statistical analyses; and M. Campbell and S. Nigra for exceptional animal care. This study was supported by grants from the National Institute on Deafness and Other Communication Disorders (J.V.B. and A.J.R.), the McKnight Endowment Fund for Neuroscience (J.J.B.) and the American Otological Society (Research Training Fellowship to S.P.G.).

Author Contributions The project was conceived by J.V.B. Experiments were planned and performed by S.P.G. and D.W.W. with advice from J.V.B., and were analysed by S.P.G., D.W.W. and J.V.B. J.V.B. performed the experimental embryology. A.J.R. conducted the electrophysiology experiments and interpreted the results. J.C.M. acquired the scanning electron micrographs. J.V.B. and A.J.R. wrote the paper.

Author Information Reprints and permissions information is available at www.nature.com/reprints. Correspondence and requests for materials should be addressed to J.V.B. (brigande@ohsu.edu).

METHODS

Expression plasmid construction. To construct pEF1 α -GFP we cut pBMN-IRES-GFP and pEF1 α -GFP with EcoRI/BsrGI to excise IRES-GFP and GFP, respectively. IRES-GFP was then ligated to the pEF1 α vector to form pEF1 α -IRES-GFP. To construct EF1 α -ZsGreen, we subcloned the *EEF1A1* promoter from pEF1 α -GFP into pGEM with the use of SalI. A plasmid with *EEF1A1* in the correct orientation was then digested with SalI/EcoRI and the promoter fragment was ligated into pZsGreen1-DR (Clontech) linearized with XhoI/EcoRI. To construct pEF1 α -Atoh1-IRES-GFP, we created the Gateway-enabled destination vector pEF1 α -RfC.1-IRES-GFP with the Gateway Vector Conversion System (Invitrogen) by digesting pEF1 α -IRES-GFP with EcoRI, blunting the ends, and inserting Reading Frame Cassette C (RfC.1). Atoh1 complementary DNA was obtained from the American Type Culture Collection (MGC-19141) and the open reading frame was amplified with the primers 5'-GGG-GACAAGTTTGTACAAAAAAGCAGGCTTAATGTCCCGCCTGCTGCAT-3' and 5'-GGGGACCACTTTGTACAAGAAAGCTGGGTACTAAGTGCCTCATCAGA-3'. A BP recombination reaction was performed with *Atoh1* cDNA and the donor vector pDONR/Zeo, creating pENTR-Atoh1/Zeo. The subsequent LR recombination reaction between pENTR-Atoh1/Zeo and pEF1 α -RfC.1-IRES-GFP generated the expression plasmid pEF1 α -Atoh1-IRES-GFP.

Expression plasmid purification. Expression plasmids were prepared with the Qiagen HiSpeed Plasmid Maxi Kit with modification. The plasmid was filtered at 0.22 μ m before precipitation with ethanol, then resuspended in sterile PBS at 3 μ g μ l⁻¹ and stored at -20 °C. Crystalline fast green was added to a freshly thawed aliquot to aid visualization during microinjection.

Timed pregnant breeding. Noon on the day on which a vaginal plug was detected was designated embryonic day 0.5 (E0.5) of development. Our initial experiments to define efficacious electroporation parameters were conducted with CD1 mice because of their fecundity. However, CD1 mice show elevated auditory thresholds by the fourth postnatal week. We outcrossed CD1 females with C57BL/6NTac males to generate CD1/B6 mice, which have normal auditory brainstem responses up to P35. Electrophysiology was conducted on hair cells in the CD1/B6 postnatal organ of Corti.

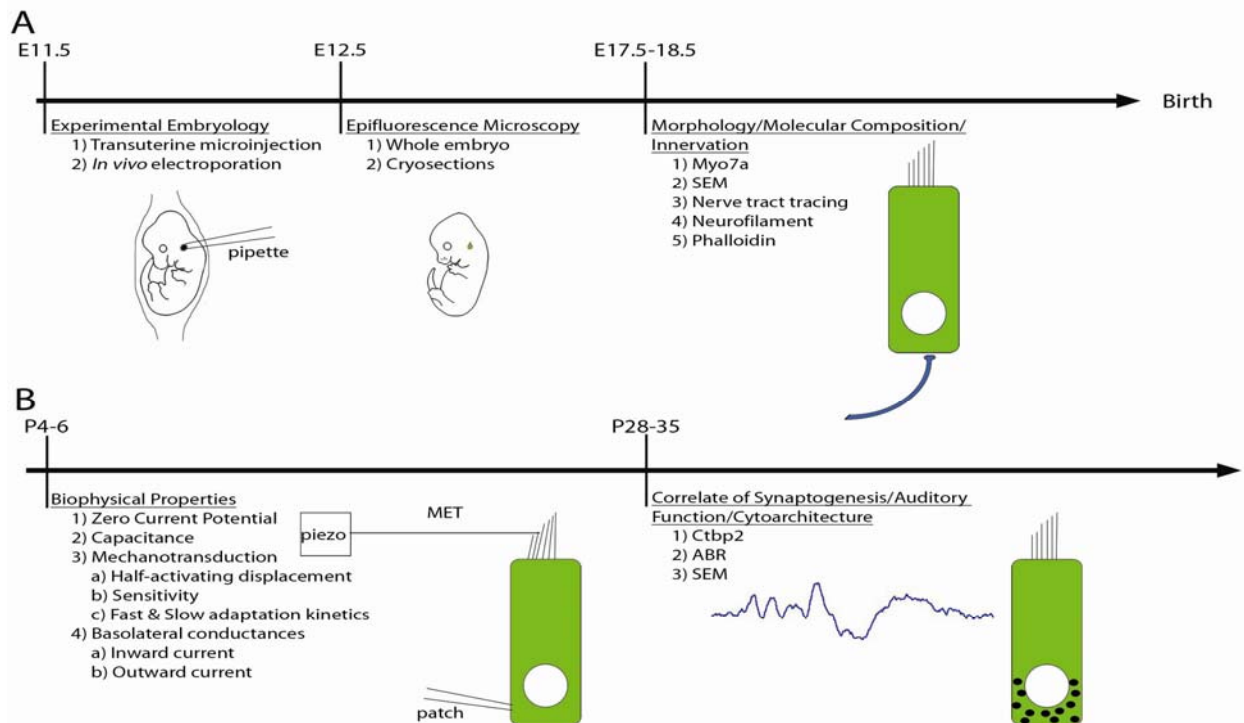
Experimental embryology. Dams were anaesthetized with 7.2 μ l per gram body weight of a solution containing 9 mg ml⁻¹ Nembutal, 20.8 mg ml⁻¹ magnesium sulphate heptahydrate, 40% propylene glycol and 10% ethanol. The bicornate uterus was externalized by ventral laparotomy. A soft-cable fibre-optic light guide was pressed lightly against the irrigated uterus to illuminate the rostral and caudal branches of the primary head vein between which the otic vesicle resides (see Supplementary Video 1). Microinjection pipettes were fabricated with an 18–24 μ m outer diameter and a 20° bevel. The pipette was advanced through the uterus and extraembryonic membranes and into the fluid-filled lumen of the otocyst. Expression plasmid tinted with fast green tracking dye was injected under pressure (about seven to nine 10-ms pulses per otocyst at about 70–103 kPa) into the lumen of the vesicle with a Picospritzer III (source gas nitrogen, 99.9% purity). The plasmid-filled otocyst was centred in the

circular 5-mm field of the tweezer-style electrode paddles by securing the uterus with a gentle grip from the cathode and anode disks. A train of five square-wave pulses (43 V per pulse at 50 ms per pulse and 950 ms interpulse delay) was delivered to drive the plasmid into ventral otic epithelial progenitors.

Immunohistochemistry. Embryos were harvested 24 h or 6–7 days after electroporation and fixed in 4% paraformaldehyde in PBS (PFA/PBS; pH 7.2–7.4) for 8–12 h at 4 °C, with gentle agitation. Postnatal mice were fixed by cardiac perfusion with PFA/PBS and inner ears were decalcified in disodium EDTA. For cryostat sections, the entire E12.5 head was cryoprotected in graded sucrose/PBS to 30%, embedded in OCT medium and serially sectioned at 12 μ m in the coronal plane. For whole mounts, the cochlea was dissected free of the cartilaginous capsule and the lateral wall was removed. The cryostat sections or dissected cochleae were permeabilized and blocked in 0.2% saponin in blocking solution (PBS containing 1% BSA and 3% serum from the species in which the secondary antibody was generated). Myo7a and neurofilament antibodies were applied overnight at 4 °C with gentle agitation. Alexa-Fluor-conjugated secondary antibody was applied for 2 h at room temperature (22 °C). Phalloidin-Alexa-Fluor conjugates were applied for 30 min at room temperature in PBS. Sectioned cochleae and the base, midbase or apex of whole-mount cochleae were covered in VectaShield (Vector Laboratories) before epifluorescence or confocal analysis. Antibodies and labelling reagents used were as follows: Alexa-660-conjugated phalloidin (dilution 1:50; A22285; Molecular Probes), Myosin 7a (dilution 1:150; 25-6790; Proteus Biosciences, Inc.), neurofilament (dilution 1:1,000; ab10586; Abcam, Inc.), Alexa 568-conjugated goat anti-rabbit (dilution 1:300; A11036; Molecular Probes) and Cy5-conjugated goat anti-chicken (dilution 1:100; ab6569; Abcam, Inc.).

Electrophysiology. Electrophysiological investigations were performed on isolated organs of Corti between P4 and P6. Tissue was isolated as described previously²⁵. Isolated tissue was placed into a coverslip-bottomed recording chamber and held in place with single strands of dental floss. The bath was perfused at a rate of 2.5 ml min⁻¹ with a solution containing (in mM): 135 NaCl, 1 KCl, 10 HEPES, 1.5 CaCl₂, 2 MgCl₂, 6 glucose, 4 pyruvate, 2 ascorbate, 2 creatine; the pH was set at 7.4 and osmolality was maintained at 325 mosmol kg⁻¹. The chamber and tissue were viewed with an Olympus BX51 microscope with the use of a \times 60 water-immersion lens and Nomarski optics (Olympus America); images were captured with a Hamamatsu C2400 camera. Hair cells were patch-clamped with an Axoclamp 200b amplifier (Molecular Devices) coupled to a 1322 Digidata A/D, D/A board (Molecular Devices) driven by JClamp software (SciSoft). Soda-glass (Garner Glass) pipettes (resistances 1–3 M Ω) coated with ski wax were used to record from both GFP⁺ and GFP⁻ cells. The internal solution contained (in mM): 125 KCl, 10 HEPES, 5 Mg-ATP, 5 creatine phosphate, 1 EGTA, 2 ascorbate; the pH was balanced to 7.2 and the osmolality was kept at 295 mosmol kg⁻¹. Mechanical stimulation was accomplished with a stiff glass probe attached to a piezoelectric stack (Physik Instrumente). Stimuli were filtered at 20 kHz (901P filter; Frequency Devices) and differentially amplified through a PA5 attenuator (Tucker Davis) to regulate stimulus amplitudes. Data were sampled at 40 kHz, filtered at 10 kHz; each stimulus is an average of eight samples. Junction potential and series resistance were corrected offline.

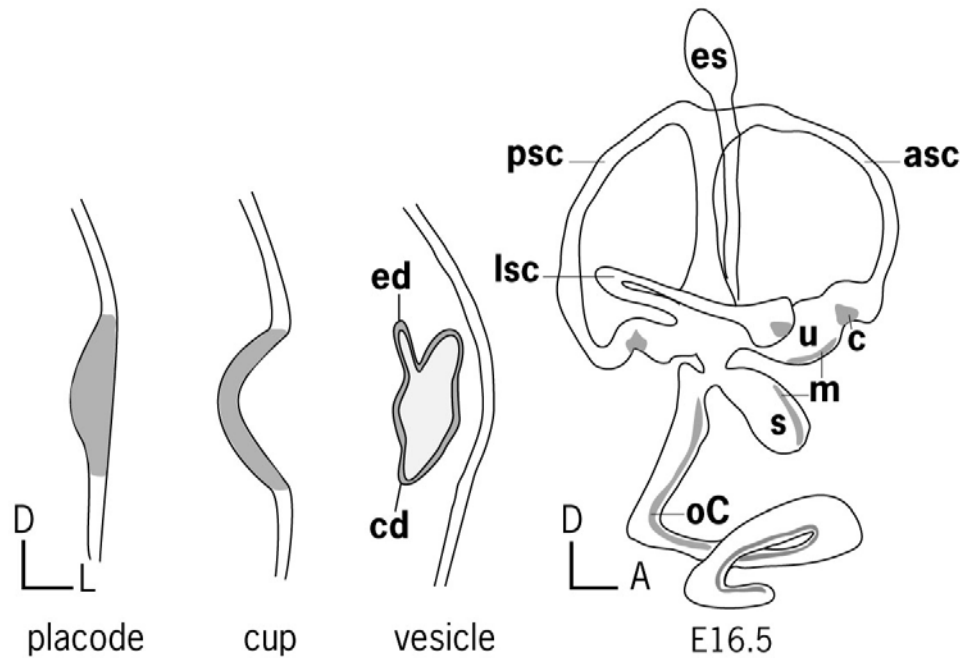
SUPPLEMENTARY INFORMATION



Supplementary Figure 1. Experimental strategy to generate sensory hair cells in the mammalian cochlea and evaluate their morphological, molecular, and biophysical properties.

A) Expression plasmid encoding GFP (control) or *Atoh1*/GFP is microinjected into the E11.5 mouse otocyst and electroporated into otic epithelial progenitor cells (E11.5). Short harvest embryos are collected at E12.5 to validate GFP expression in the whole embryo and in cryosections of the otocyst. Long harvest embryos are collected 6-7 days post-electroporation (E17.5-18.5) to evaluate morphological and molecular properties of hair cells: 1) Myosin 7a (*Myo7a*) expression by immunohistochemistry on cochlear whole mounts; 2) stereociliary bundle morphogenesis by scanning electron microscopy (SEM); 3) innervation by retrograde labeling of nerve tracts originating in the cochlear nucleus; 4) neurofilament expression by

immunohistochemistry on cochlear whole mounts; and 5) stereociliary bundle morphogenesis by whole mount phalloidin staining. B) A series of embryos whose inner ears were injected and electroporated with the GFP or Atoh1/GFP constructs at E11.5 are selected for at birth. On postnatal day 4-6 (P4-6), the listed biophysical properties are evaluated. On postnatal day 28-35 (P28-35), immunohistochemistry on cryostat sections of decalcified cochlea is conducted for the ribbon synapse marker, C-terminal binding protein 2 (Ctbp2). SEM is conducted to assess the cytoarchitecture of Atoh1/GFP-transfected ears. Auditory brainstem response thresholds (ABR) are determined on adult mice that had been electroporated at E11.5 to assess the effect of *in vivo* electroporation on the acquisition of hearing.



Supplementary Figure 2. Morphogenesis of the Mouse Inner Ear

The inner ear develops from a thickened patch of head ectoderm called the otic placode (gray), which invaginates to form the otic cup. Over approximately 2 days in mice, the cup cinches together to establish the fluid-filled otic vesicle or otocyst. The otic vesicle is a convenient target for microinjection since it is superficially located just beneath the head ectoderm. The injected expression plasmid is contained within the vesicle by the otic epithelium. The endolymphatic duct (ed) emerges from the dorsomedial portion of the vesicle and the cochlear duct (cd) from the ventromedial region. By embryonic day 16 (E16.5), the shape of the inner ear closely resembles that of the fully mature, postnatal inner ear. The anterior, posterior, and lateral semicircular canals (asc, psc, and lsc, respectively) are formed by the fusion of the epithelial walls of the canal pouches with subsequent sculpting by programmed cell death. There are 5 vestibular sensory epithelia consisting of hair cells and supporting cells: 3 cristae (c) in the ampullae of the semicircular canals and 2 maculae (m) in the utricle (u) and saccule (s). The

auditory sensory epithelium is located in the organ of Corti (oC) within the coiled cochlea and in mammals displays one row of inner hair cells and three rows of outer hair cells. Our experiments involved transuterine microinjection of expression plasmid into the E11.5 otocyst; electroporation-mediated gene transfer to otic epithelial progenitors giving rise to the organ of Corti; and analyses of transfected otocysts or cochleae 24hrs, 6-7 days (E17.5-18.5), or 35-42 days (P28-35) post-electroporation. Abbreviations: A, anterior; D, dorsal; es, endolymphatic sac; L, lateral. Images are not to scale.

Supplementary Table 1: Auditory brainstem response (ABR) thresholds of postnatal day 28-35 mice that were subjected to transuterine microinjection of expression plasmid and *in vivo* electroporation at embryonic day 11.5

Strain/Phenotype	Construct/Otocyst Injected	Electroporated*	ABR		n	4KHz [†]	8KHz	16KHz	32KHz
			Ear(s)						
C57BL/6NTac	Not applicable (n/a)	no	both		17	68 ± 4.4	65 ± 5.6	44 ± 6.1	48 ± 3.6
CD1x C57BL/6NTac	n/a	no	both		29	67 ± 5.9	67 ± 4.7	45 ± 6.7	58 ± 24
No expression [§]	pEF-Atoh1-GFP or pEF-GFP/Left	yes	both		15	70 ± 8.1	66 ± 3.7	44 ± 6.4	54 ± 10
GFP expression	pEF-GFP/Left	yes	left		4	67 ± 4.1	64 ± 4.1	47 ± 2.5	56 ± 11
Contralateral	n/a	yes	right		3	73 ± 2.9	62 ± 2.9	45 ± 2.9	52 ± 5.0

* electroporation parameters: 43V, 50 msec/pulse, 950msec interpulse delay, 5 pulses total.

[†] means ± the standard deviation of the mean were compared by ANOVA with Bonferroni post-hoc test; no differences were found.

[§] all electroporated embryos are CD1 outcrossed to C57BL/6NTac (CD1xC57BL/6NTac).

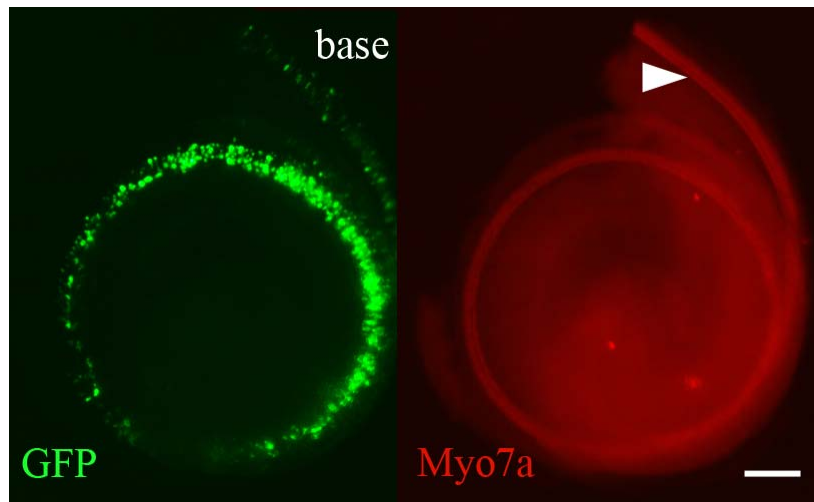
Explanation of Supplementary Table 1

The efficacy of *in utero* gene transfer hinges upon the elaboration of appropriately patterned maternal behavior after survival surgery. The outbred CD1 mouse strain is fecund, tolerates invasive procedures exceptionally well, and displays uncompromised maternal behavior post-surgically. However, the CD1 strain also presents with hearing loss postnatally and does not represent the ideal strain for longitudinal studies of auditory function. We therefore outcrossed CD1 females to C57BL/6NTac males to generate the CD1xC57/BL6NTac mice that have normal ABR thresholds at postnatal day 28-35. This breeding paradigm allows us to take advantage of the maternal CD1 strain characteristics while conducting gain-of-function studies in offspring that have normal ABR thresholds.

No expression control: Left ears were injected with either the Atoh1-GFP or the control GFP construct, electroporated, but did not express GFP postnatally. ABR thresholds were normal.

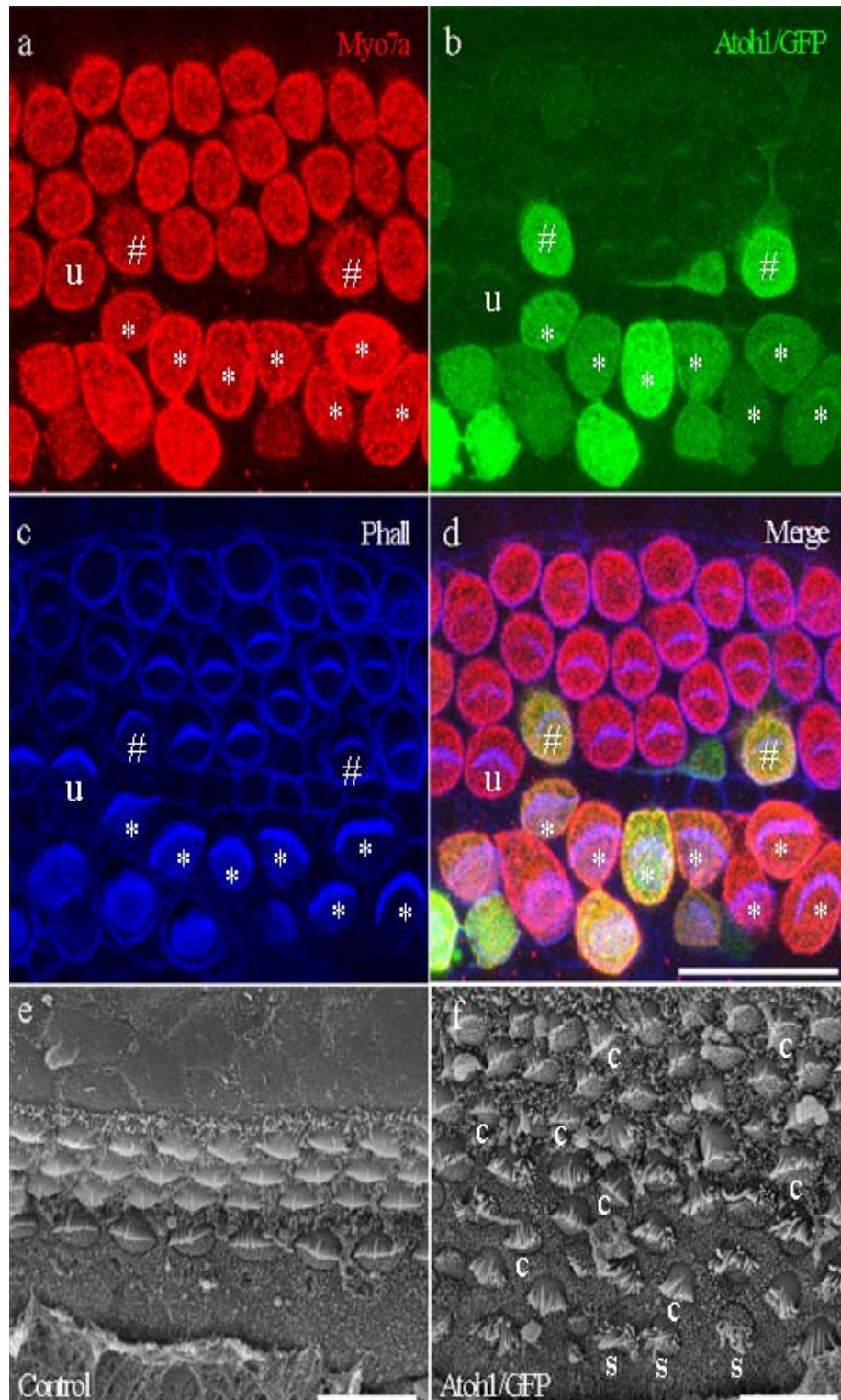
GFP expression control: Left ears were injected with the GFP construct whose expression was detected postnatally. Thresholds were normal.

GFP expression control: Contralateral: The right (contralateral) ears from the GFP expression control mice were evaluated independently. The right ears are closer to the anode, a variable we sought to investigate. ABR thresholds were normal. One ear was excluded due to a data storage error during recording.



Supplementary Figure 3. *In vivo* electroporation transfects progenitors that give rise to the organ of Corti.

The EF1 α -GFP expression construct was injected and electroporated into the embryonic day 11.5 mouse otocyst. The distribution of GFP in the inner ear 7 days post-electroporation (GFP, left) grossly followed the distribution of the hair cell marker, myosin 7a (Myo7a, right). The arrowhead indicates the 4 rows of Myo7a⁺ sensory hair cells that extend from the base to the apex of the organ of Corti. These data suggest that *in vivo* electroporation transfects progenitors that give rise to the organ of Corti but does not alter the gross morphogenesis of the inner ear. Scale bar: 100 μ m.



Supplementary Figure 4. Stereociliary bundle morphology and cochlear patterning in late embryonic, *Atoh1*/GFP-transfected cochlea. The EF1 α -*Atoh1*-IRES-GFP expression construct was

injected and electroporated into the embryonic day 11.5 mouse otocyst. Stereociliary bundle morphology and cochlear patterning were analyzed at embryonic day 18.5 by whole mount phalloidin staining (n = 18 cochleae) and at embryonic day 17.5 by scanning electron microscopy (n = 3 cochleae). Phalloidin⁺ apical epithelial protrusions were detected in Atoh1/GFP⁺/Myosin7a⁺ cells in the inner (marked with white asterisks) and outer (marked with the white number symbol) rows of hair cells (panels a-d). The bundles appeared well consolidated with no gross evidence of dysmorphogenesis (i.e., splaying or toppling). An untransfected, phalloidin⁺/Myo7a⁺ hair cell (marked with the letter “u”) is labeled for comparison (panels a-d). The polarity of the bundles on supernumerary hair cells was frequently skewed, however. Scanning electron micrographs of the Atoh1/GFP-transfected inner ear demonstrated a grossly mispatterned organ of Corti with supernumerary hair cells displaced in a broadened mediolateral band of the cochlear duct (panel 4f). Bundles were present on the supernumerary hair cells, and in many cases their shape was consistent with the control bundles (representative bundles are marked with the letter “c”). Some hair cells proximal to the modiulus displayed bundles that appeared splayed (marked with the letter “s”). Scale bars: a-d, 20 μm; e,f: 10 μm.

Supplementary Table 2: Mean number of hair cells, transfected hair cells, and transfected supporting cells per 100 micron field in the base, midbase, and apex of GFP and Atoh1/GFP-transfected cochleas at E 18.5

Cells Counted (molecular phenotype)	Mean Number of Cells per 100 μ m Field [†]		
	Base	Midbase	Apex
Total Number of Hair Cells			
(Myo7a ⁺) [§]			
GFP	106 \pm 2.7	122 \pm 3.0	131 \pm 2.2
Atoh1/GFP	193 \pm 24	143 \pm 7.6	137 \pm 8.8
	p=0.021*	p=0.021	p=0.724
Inner Hair Cells			
GFP	24 \pm 0.8	28 \pm 0.8	31 \pm 0.9
Atoh1/GFP	53 \pm 8.1	45 \pm 2.5	37 \pm 6.5
	p=0.021	p=0.021	p=0.773
Outer Hair Cells			
GFP	82 \pm 2.0	94 \pm 2.3	101 \pm 1.7
Atoh1/GFP	126 \pm 24	98 \pm 7.5	100 \pm 2.4
	p=0.043	p=0.885	p=0.773
Outer/Inner Ratio			
GFP	3.4	3.4	3.3
Atoh1/GFP	2.4	2.2	2.7
<hr/>			
Total Number of Transfected Hair Cells			
(GFP ⁺ /Myo7a ⁺)			
GFP	15 \pm 5.7	16 \pm 7.0	5.9 \pm 2.4
Atoh1/GFP	100 \pm 41	60 \pm 12	49 \pm 23
	p=0.021	p=0.021	p=0.043
Transfected Inner Hair Cells			
GFP	4.0 \pm 1.5	5.6 \pm 1.4	1.6 \pm 0.4
Atoh1/GFP	41 \pm 10	35 \pm 3.8	21 \pm 11
	p=0.021	p=0.021	p=0.139
Transfected Outer Hair Cells			
GFP	11 \pm 4.2	11 \pm 5.9	5.5 \pm 1.7
Atoh1/GFP	50 \pm 33	25 \pm 11	29 \pm 12
	p=0.191	p=0.149	p=0.080
Outer/Inner Ratio			
GFP	2.8	2.0	3.4
Atoh1/GFP	1.2	0.7	1.4
<hr/>			
Total Number of Transfected Supporting Cells			
(GFP ⁺ /Myo7a ⁻)			
GFP	69 \pm 11	58 \pm 15	16 \pm 5.2
Atoh1/GFP	64 \pm 29	46 \pm 16	12 \pm 3.8
	p=0.248	p=0.773	p=0.386

[†] Mean \pm the standard error of the mean; n=4

[§] Myosin 7a

* Mann-Whitney U test comparing GFP and Atoh1/GFP means within region.

Supplementary Video 1

This movie shows microinjection of expression plasmid into the left otic vesicle of an embryonic day 11.5 mouse embryo. The microinjection pipette delivers approximately 200nL of plasmid solution to the otocyst. Note the pulsing blood flow in the visceral yolk sac vasculature (central foreground). The uterus has been resected to acquire clear video images, though the experimental injections are performed with the uterus intact. The narrow, dorsal endolymphatic duct and the tapered, ventral cochlear duct (Supplementary Figure 2) are clearly evident after the injection is completed (QuickTime; 2.5MB).

Supplementary Video 2

This movie shows an embryonic day 11.5 mouse embryo electroporated with paddle style electrodes. The left otocyst was filled with expression plasmid by transuterine microinjection and the narrow, dorsal endolymphatic duct is evident. The otocyst is centered between the cathode (lateral to the injected otocyst) and anode (lateral to the contralateral, uninjected otocyst) by applying gentle compression. The successful completion of the square wave pulse train generates bubbles on the surface of the irrigated uterus (QuickTime; 10.5 MB).

Supplementary Video 3

This video shows a 360 degree view of an Atoh1/GFP-transfected, embryonic day 18.5 mouse organ of Corti immunostained for myosin7a (Myo7a; red) and neurofilament (blue). 4 Atoh1/GFP⁺/Myo7a⁺ cells are present in the bottom portion of the frame and the first row of outer hair cells is located in the upper portion. The 3-dimensional reconstruction shows that the blue neurofilament⁺ processes associate with the base of GFP⁺ and GFP⁻ cells that express Myo7a (QuickTime; 6.2 MB).

Supplementary Video 4

This video shows a 360 degree view of a cryosection from an Atoh1/GFP-transfected, postnatal day 35 organ of Corti immunostained for Myo7a (blue) and C-terminal binding protein 2 (Ctbp2; red). The 2 hair cells on the left appear closely juxtaposed and are GFP⁺. The cell in the middle has weak GFP expression and the cell on the right is GFP⁻. The 3-dimensional reconstruction shows Ctbp2 distribution in the basal and basolateral domains of all of the Myo7a⁺ cells (QuickTime; 2.4 MB).

Efficacy of transuterine microinjection and *in vivo* electroporation. Microinjection of expression plasmid into the E11.5 otocyst without electroporation carries a 90% survival rate provided that microinjection pipette tip geometry, bevel angle, and taper rate are rigorously constrained. In our most recent round of *in utero* gene transfer experiments to support these studies (i.e., the “rebuttal ears”), we conducted 13 surgeries on CD1 dams: 75 total E11.5 inner ears from the 13 dams were injected and electroporated; 45 embryos survived to the E17.5 harvest time point (60%); 17/45 (38%) were transfected with expression construct. Only one ear was weakly transfected (sporadic GFP⁺ cells in the cochlear base), and the remaining 16 were strongly transfected (bright GFP expression in 2 of 3 cochlear turns) or robustly transfected (bright GFP expression in the base, midbase, and proximal apex). Seventeen informative, transfected inner ears out of 75 injected is 23% efficiency overall, which compares favourably to the yield of homozygous recessive mouse mutants from a conventional heterozygous breeding paradigm. We perform 2-4 surgeries per day averaging 1.4 hrs per mouse which includes pre-operative protocols and the complete *in utero* gene transfer procedure (i.e., ventral laparotomy, transuterine microinjection and electroporation of 4-6 embryos, and survival surgery log documentation). Post-operative monitoring and documentation for the group of dams typically involves an additional 1.5-2 hrs.